

# EFFECTS OF TEMPERATURE ON EQUIVALENT ELASTIC AND CREEP DEFORMATION BEHAVIORS OF A DRIED SAND

Yodphao Punya-in<sup>1</sup>, and Warat Kongkitkul<sup>2,\*</sup>

<sup>1,2</sup>Department of Civil Engineering, Faculty of Engineering,  
King Mongkut's University of Technology Thonburi, Thailand

\*Corresponding Author, Received: 30 Nov. 2021, Revised: 28 Dec. 2021, Accepted: 13 Jan. 2022

**ABSTRACT:** Granular materials, e.g., sand, may be subjected to changes in the ambient temperature while supporting typical working stress. As a result, their elastic and long-term creep deformation behaviors may be altered by the temperature change. In this study, an automated triaxial loading system that can accurately control both the loading and temperature histories was developed. A series of special triaxial compression tests using an air-dried sand sample was performed. The temperature surrounding the sample was varied from 30 °C to 60 °C and controlled constant for subsequent shearing by axial compression. The shearing was performed using various loading histories consisting of: i) continuous monotonic loading (ML); ii) sustained (creep) loading (SL); and iii) cyclic loading (CL) with small amplitude. The following are found from the results of this study. The peak and residual shear strengths tend to decrease with increasing temperature. The equivalent elastic Young's modulus increases with increasing stress level in a hypo-elasticity manner, but at the same stress level, it decreases significantly with increasing temperature. Creep strain is obvious and it increases with increasing stress level and temperature.

*Keywords: Shear strength, Elastic, Creep, Temperature, Sand*

## 1. INTRODUCTION

In several geological and geotechnical engineering projects such as nuclear waste repositories [1], high voltage electric cables [2], energy piles [3-5], thermally-active embankments [6], thermally-active retaining walls [7], geothermal tunnel linings [8], highway pavements [9], geosynthetic reinforced soil (GRS) structure [10], the soils are subjected to non-isothermal conditions [11]. That is, the ambient temperature surrounding them changes cyclically or arbitrarily. Therefore, for such a circumstance, it is necessary to understand the stress-strain behaviors, which are affected by the change in the temperature. In the literature, the thermal effects on the yield stress of clays have been widely investigated throughout temperature-controlled conditions such as triaxial compression test, one-dimensional compression test, and isotropic compression test [12-15].

The deformation characteristics of granular material (i.e., gravel and sand) at a small-strain level are important for many geotechnical engineering problems. For instance, they are necessary for a precise prediction of the settlement of the foundation supporting a megastructure or the ground movement caused by a deep excavation. In such cases, strains mobilized in the ground by working loads are usually smaller than about 0.1%, or at the largest, about 0.5% [16, 17]. At such a small-strain level, the soil behaviors are significantly elastic, and therefore the

elastic deformation properties, i.e., the elastic stiffness, are essential design parameters.

The dependency of elastic properties of geomaterials on various factors has been investigated by many researchers. For example, Kohata [18] performed a series of triaxial compression tests on the Hostun sand sample employing a comprehensive loading history (e.g., cyclic loading during otherwise monotonic loading) and showed that the elastic deformation characteristics of granular materials depend on the stress state. Hitcher [19] investigated the elastic properties of various soil types (e.g., sand, gravel, clays) by subjecting them to very small strains in triaxial compression and extension. Elasticity was found to be nonlinear because the elastic modulus depends on the mean effective stress in a nonlinear manner. Although there are many studies on the dependency of elasticity on the stress-state in the literature, little has been attempted to investigate the effect of temperature on the elasticity of granular materials, especially for sands.

On the other hand, it is known that geomaterials also exhibit creep deformation upon sustained loading. Creep deformation depends on soil type, stress level, and so on. Tatsuoka [20] explained that creep is a deformational response due to the material viscous properties, and can be explained by a non-linear three-component model, by which creep depends on the initial strain rate, viscosity type, rate-sensitivity, stress level, and decay characteristic. The study by Lu [21] showed that the change of

temperature could affect the creep deformation of saturated marine deposits. Understanding creep deformation is an important key for predicting the long-term deformation of foundations of megastructures, whereas the immediate settlement can be predicted by the elastic properties. Nevertheless, to the best of the authors' knowledge, little has been known on how the temperature alters the creep deformation of geomaterials, especially with the dried sand.

Among the limitedly available studies on the temperature effects on sands, most of them focused only on the shear strength behaviors. For instance, Liu [22] performed hollow cylinder tests on Fujian standard quartz sand samples. The sample was heated under a drained condition, then isotropically consolidated, and finally sheared under an undrained condition. Their test results showed that the shear-induced pore pressure of the heated quartz sand greatly increased, thus weakening the shear strength. He [23] performed another test on calcareous sand to compare it with Fujian standard quartz sand. The sample was heated under a drained condition, subjected to  $K_0$  consolidation, and then sheared under a drained condition. Their results showed that with increasing the temperature, the strength and dilatancy of the quartz sand are improved, but the opposite was found with the calcareous sand. This is because an increase in the temperature aggravated the particle breakage for the calcareous sand during shearing, while for the quartz sand, the discharge of pore water and the densification.

## 2. RESEARCH SIGNIFICANCE

As mentioned in the previous section, it can be seen that when working under non-isothermal conditions, the elastic and long-term creep deformation behaviours, as well as the shear strength of soils, can be altered by the change in temperature. Consequently, this paper aims to study temperature effects on elasticity and stress-strain deformation behaviors of sand by performing a series of special triaxial compression tests. An air-dried sample was used so that the complexity of setting up the triaxial loading system with a temperature control unit was minimized. This was also to avoid pore pressure induced by the heating, consolidation, and shearing stages. The sample once erected was subjected to heat until reaching the target temperature, after which held constant thorough the test. During the above-mentioned three stages, the sample was allowed to drain by connecting the specimen's inside to the atmosphere. The stress-strain deformation behaviors were studied by subjecting the sample to various loading patterns (i.e., monotonic loading, sustained loading, cyclic loading) under different constant controlled temperatures.

## 3. TEST APPARATUS AND MATERIAL

### 3.1 Test Apparatus

A new temperature-controlled triaxial test apparatus shown in Fig. 1 has been developed in the present study. It consists of: i) a cylindrical cell of which the cell water pressure is automatically controlled by an electro-pneumatic (E/P) transducer and the cell water temperature by the temperature control unit; and ii) an automatic axial loading system with precise gear. The newly developed temperature control unit consists of a heater, a temperature controller unit, and a circulating pump. A temperature transducer (k-type thermocouple) was installed inside the triaxial cell and connected to a computer for recording. Complicated shear loading histories (e.g., small-strain cyclic loading, creep) can be successfully performed by the precise gear loading system, which can respond sharply to control the loading directions and the speed [24]. After finishing the specimen preparation, the triaxial cell was then sealed and connected to the temperature control unit. Next, the cell water temperature was elevated to the target value by circulating the water throughout a heater located outside. The heater is automatically controlled by the temperature controlling unit. After achieving the target value, the temperature was maintained constant with an accuracy of  $\pm 0.5$  °C, as shown in Fig. 2.

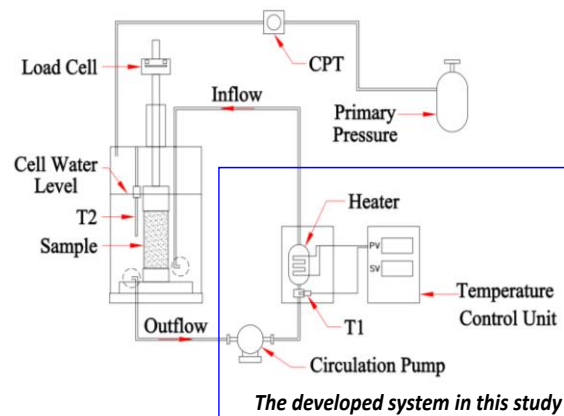


Fig. 1 Temperature-controlled triaxial test apparatus newly developed

### 3.2 Test material

A river bed sand in Thailand was used as the test material in the present study. It was treated by sieving and only the portion that passed through the sieve no. 40 but retained on the sieve no. 100 was used. Then, it was cleaned by flushing with tap water to remove any remaining fines attracted on the particle's surface, and then oven-dried. This sand is sub-angular in grain shape. It has a specific gravity ( $G_s$ ) of 2.640, an effective particle size ( $D_{50}$ ) of 0.285 mm, and a coefficient of uniformity ( $C_u$ ) of 1.879. The

maximum and minimum void ratios are 1.035 and 0.665, respectively.

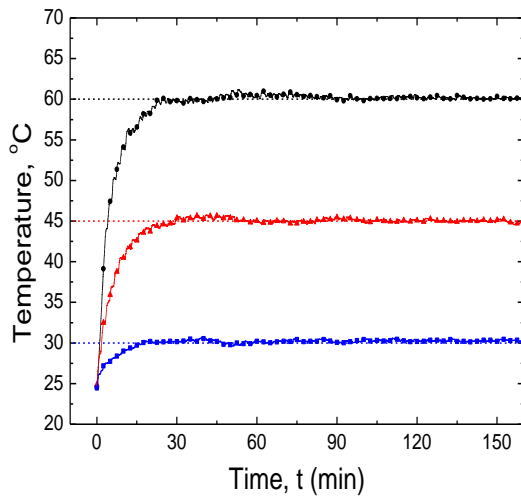


Fig. 2 Typical time histories of the measured temperature of the cell water

## 4. TEST METHOD

### 4.1 Specimen Preparation

The top cap and pedestal were lubricated with a 50- $\mu\text{m}$  thick high-vacuum silicone grease layer adhered with a 0.3-mm thick natural latex sheet. A split mold with an inner diameter of 70 mm and a height of 150 mm was used to prepare the test sample. After adhering to the membrane with the mold and being placed on the pedestal, the sand was filled in by using the air pluviation technique [25] using a multiple-sieving apparatus to achieve high uniformity. The relative density in a range of 88 - 95 % was achieved by this method. Table 1 lists the values of the initial void ratio ( $e_0$ ) and thus initial relative density ( $D_{r0}$ ) for all the test specimens.

After sealing the membrane with the top cap, a partial vacuuming with 20 kPa was applied to the specimen to be able to remove the mold. The specimen was then waited for reaching an equilibrium stage for 30 min (Fig. 3a)). After sealing the triaxial chamber, the partial vacuuming was replaced by the cell water pressure by gradually increasing the cell water pressure and reducing the partial vacuuming at the same time until the cell water pressure reached 20 kPa. After that, the specimen was further isotropically consolidated until the confining pressure reached 30 kPa (Fig. 3b)). By maintaining the cell pressure constant at 30 kPa, the cell water was then circulated to the heater of the temperature control unit until reaching the target temperature. Another waiting period of 90 min was employed for allowing the specimen to achieve an equilibrium stage, and then the shearing process commences while holding the cell water temperature constant.

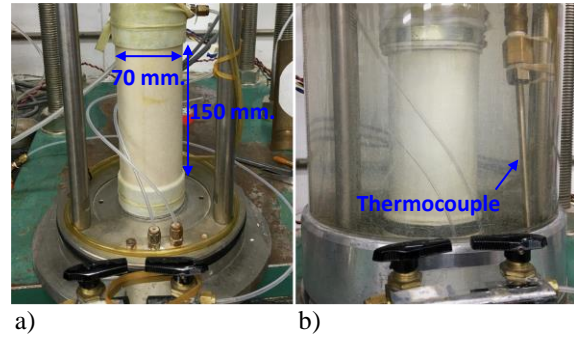


Fig. 3 Preparation of the sand sample for triaxial compression test upon a) applying a partial vacuuming of 20 kPa, and b) having been isotropically consolidated by the cell water pressure of 30 kPa.

### 4.2 Test Program

In this study, a comprehensive series of shear loading histories were employed to investigate the elastic and creep deformation behaviours of the test sand. The details are listed in Table 1 and shown in Fig. 4, which can be described as follows.

Loading type a)-ML: Continuous monotonic loading (ML) is performed at a constant strain rate of 0.03 %/min.

Loading type b)-SL-CL: ML with the strain rate of 0.03%/min is performed until reaching the target stress ratio ( $R$ ), after which the sustained loading (SL) is held for three hours for allowing the test specimen to exhibit creep deformation. At the end of SL, the specimen is considered behaves significantly only elastic behavior, by which cyclic loading (CL) with a double deviator stress amplitude ( $\Delta q$ ) of 15 kPa (or equal to  $\Delta R$  of 0.5) is applied for 10 cycles for evaluating the quasi-elastic Young's modulus ( $E_{eq}$ ). After finishing CL, ML is restarted to the next target  $R$ -value. For this loading type, the target  $R$  values are equal to 2.0, 3.5, and 5.0.

Loading type c)-SL-CL: This loading type is the same as the loading type b), except the values of target  $R$  are equal to 2.75, 4.25, and 5.75. It is worthy to note that loading types b) and c) are the same in the manner how the SL and CL are applied. The difference is that, under a controlled temperature, SL and then CL is applied at  $R = 2.0, 3.5, \text{ and } 5.0$  for loading type b) in a single test and at  $R = 2.75, 4.25, \text{ and } 5.75$  in the other single test, as shown in Fig. 4.

For each loading type mentioned above, the cell water temperature surrounding the test specimen is controlled constant at either 30 °C, 45 °C, or 60 °C throughout the shearing process. This range of temperature is consistent with the values used in the studies with sands by Liu [22] and He [23]. In addition, there was also a limitation of the triaxial loading system used in the present study in that: i) there was no system to cool down the temperature

below the room temperature; and ii) the maximum temperature was limited at 60 °C for avoiding any damage to the measuring devices (e.g., pressure transducer).

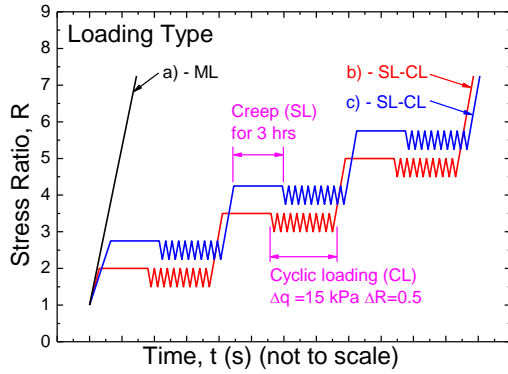


Fig. 4 Illustration of time histories of stress ratio ( $R$ ) for loading types a), b) and c) according to the test program.

Table 1 Triaxial compression test program with different shearing histories and different temperatures

Test No.	$e_0$ (-)	$D_{r0}$ (%)	Loading Type	$T$ (°C)	Target $R$
1	0.686	94.39	a)-ML	30	-
2	0.695	92.02	a)-ML	45	-
3	0.707	88.52	a)-ML	60	-
4	0.703	89.73	b)-SL-CL	30	2.0, 3.5, 5.0
5	0.717	85.87	b)-SL-CL	45	2.0, 3.5, 5.0
6	0.714	86.72	b)-SL-CL	60	2.0, 3.5, 5.0
7	0.689	93.41	c)-SL-CL	30	2.75, 4.25, 5.75
8	0.683	95.10	c)-SL-CL	45	2.75, 4.25, 5.75
9	0.691	93.05	c)-SL-CL	60	2.75, 4.25, 5.75

## 5. TEST RESULTS AND DISCUSSION

### 5.1 Effect of Temperature on Shear Strength

Fig. 5 shows the relationships between the stress ratio ( $R$ ) and axial strain ( $\varepsilon_a$ ) obtained with loading type a)-ML for different temperatures. With increasing temperature surrounding the test specimen, the  $R - \varepsilon_a$  relationships observably degrade. The shear strength of the test sand can be expressed in terms of internal friction angles at the peak state,  $\phi_{peak}$ , from  $R$  at the peak state, and at the residual state,  $\phi_{res}$ , from  $R$  at the residual state defined at the  $\varepsilon_a$  equal to 12%. Due to the sand used in the experiment being very clean without any fines, the cohesion was assumed null. Thus the internal friction angle can be determined from the test employing only a single value of confining pressure as shown in Eq. (1). The values of the  $R$  and  $\phi$  at the peak and residual states are listed in Table 2. It can be seen that both  $\phi_{peak}$  and  $\phi_{res}$

tend to decrease with increasing temperature. In addition, it may be seen from Fig. 5 that not only the shear strength but also the stiffness of the  $R - \varepsilon_a$  relationship decreases with an increase in the temperature. This issue is discussed in detail later in this paper.

$$\phi = \sin^{-1} \left( \frac{R-1}{R+1} \right) \quad (1)$$

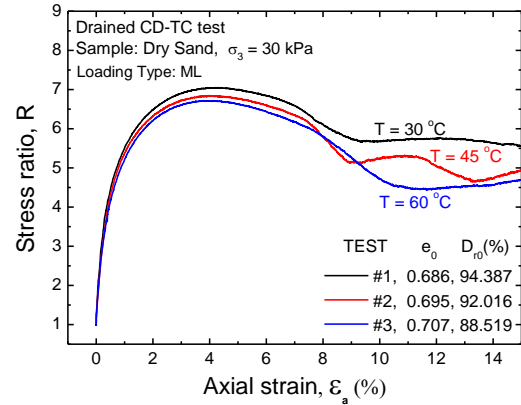


Fig. 5  $R - \varepsilon_a$  relationships for different constant temperatures with loading type a)-ML.

Table 2 Strengths of the test sand obtained from ML with different constant temperatures

$T$ (°C)	$R_{peak}$ (-)	$\phi_{peak}$ (deg.)	$R_{res}$ (-)	$\phi_{res}$ (deg.)
30	7.052	48.73	5.752	44.73
45	6.849	48.18	5.067	42.09
60	6.720	47.81	4.465	39.35

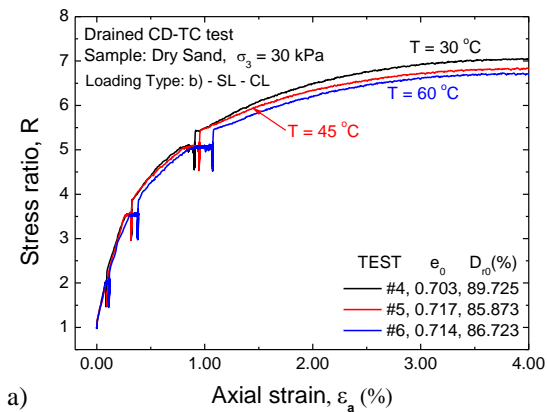
### 5.2 Stress-strain Relationships during Cyclic Loading

Fig. 6(a) and 6(b) show the relationship between  $R$  and  $\varepsilon_a$  for different constant temperatures with loading type b)-SL-CL and c)-SL-CL, respectively. In these tests, CLs were performed by unloading-reloading for 10 cycles with a small stress-amplitude ( $\Delta q$ ) of 15 kPa at different specified  $R$  values, applied after SL has been completed, during otherwise ML at a constant strain rate. The trends of  $R - \varepsilon_a$  behaviors from loading types b) - SL-CL and c) - SL-CL can be described as follows.

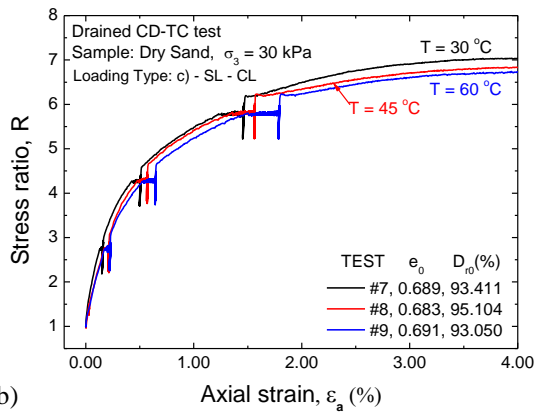
1. The  $R - \varepsilon_a$  relationships for different temperatures tend to rejoin to the respective ones that could be obtained by continuous ML tests without intermission of SL and CL. This importantly implied that the peak shear strength is maintained, while is not degraded with SL and CL applied at the pre-peak loading history. Thus, it can be postulated that although creep strain is obvious, it does not degrade the shear strength,

unlike the temperature.

2. The  $R$ - $\varepsilon_a$  relationships immediately after the restart of ML at the end of CL show a very high stiffness, which is very close to the elastic stiffness.
3. For the same temperature, creep deformation increases with increasing  $R$ -value. That is, SL performed at the stress state nearer to the failure results in more creep deformation. Most interestingly, for the same  $R$ -value, creep deformation increases with an increase in temperature.



a)



b)

Fig. 6  $R - \varepsilon_a$  relationships for different constant temperatures with: a) loading type b) - SL-CL; and b) loading type c) - SL-CL

### 5.3 Elastic Stiffness

#### 5.3.1 Determination of elastic stiffness

Fig. 7 shows an enlarged portion of Fig. 6a) around the  $R$ -value equal to 5.0. In this figure, the  $R$ -value presented on the vertical axis was converted to the major principal stress ( $\sigma_1$ ). This figure shows typical stress-strain characteristics during SL and then CL as well as upon the restart of ML at the end of CL of the present study. It can be observed that the behavior during small unload-reload cycles is highly linear-elastic, as noted by the facts that: i) the stress-

strain loops generated during the respective unload-reload cycles are very small, exhibiting negligible energy dissipation; and ii) the residual strain developed by the respective unload-reload cycles was very small.

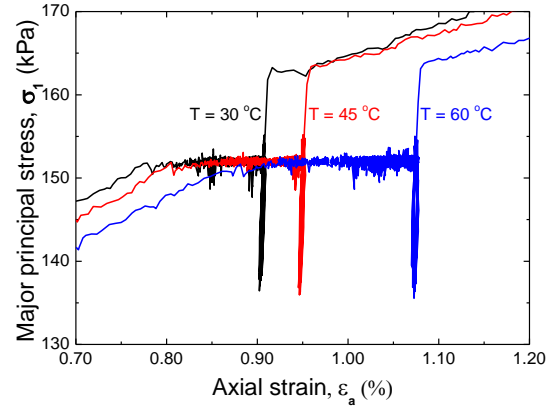


Fig. 7 Enlarged portion of Fig. 6a) showing  $\sigma_1 - \varepsilon_a$  relationships at  $R = 5.0$ .

Fig. 8a) - 8c) show the last five unloading  $\sigma_1 - \varepsilon_a$  branches by CLs at  $R$  of 5.0 (Fig. 7) for different temperatures of 30°C, 45°C, and 60°C, respectively. It can be seen from these figures that the unloading branches exhibit a highly linear-elastic behavior for the whole stress amplitude (15 kPa). Thus, it is relevant to evaluate the equivalent elastic Young's modulus ( $E_{eq}$ ) from a linear relation fitted to the respective portions of the unloading  $\sigma_1 - \varepsilon_a$  branches presented in Fig. 8. The value of  $E_{eq}$  is fairly constant during the last five unload-reload cycles for the respective CL stages. This fact indicates that the deformation during these unloading  $\sigma_1 - \varepsilon_a$  branches are essential elastic.

#### 5.3.2 Effects of stress level and temperature on the elastic stiffness

The averaged  $E_{eq}$  and  $\sigma_1/\sigma_0$  relationships were then plotted in the full-log scale for respective temperatures as shown in Fig. 9. Here,  $\sigma_0$  is the reference stress equal to 100 kPa. It can be seen that  $E_{eq}$  is not constant but increases with an increase of  $\sigma_1/\sigma_0$  ratio. The dependency of elastic modulus on the stress level can be expressed with hypo-elasticity expressed by Eq. (2). Concerning the hypo-elastic properties, the trend that the elastic stiffness of geomaterial increases with an increase in the major principal stress for which the elastic modulus is defined has been observed in triaxial tests of many types of unbound geomaterial [26-28]. The lines were best fitted to the test data points, and the values of  $E_0$  and  $m$  for respective temperatures are shown in Fig. 9a). With different temperatures, the  $E_{eq} - \sigma_1/\sigma_0$  relationships exhibit the same trend of behaviors. For the same value of the  $\sigma_1/\sigma_0$  ratio, it is noticed that the  $E_{eq}$  decreases with increasing temperature.

$$E_{eq} = E_0 \left( \frac{\sigma_1}{\sigma_0} \right)^m \quad (2)$$

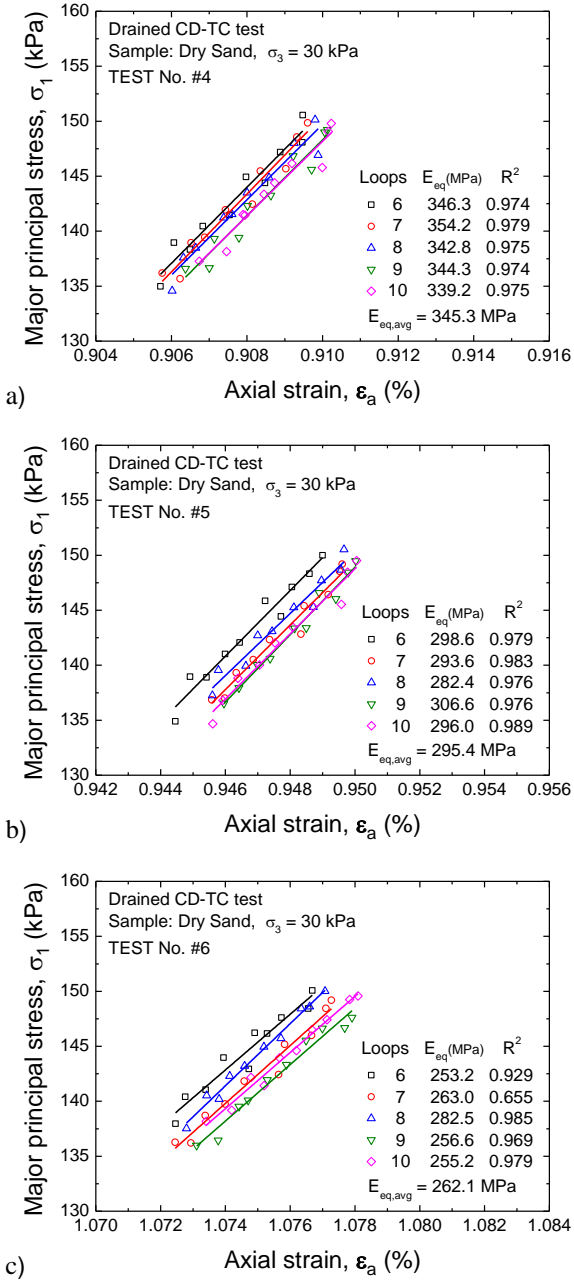


Fig. 8 Determination of equivalent elastic Young's modulus ( $E_{eq}$ ) from unloading branches of small-amplitude unload-reload cycles at  $R = 5$  presented in Fig. 7 for temperatures equal to a) 30 °C; b) 45 °C; and c) 60 °C.

Considering the  $m$  value, it could be seen that the values obtained from the tests with different temperatures are quite similar. This implies that the characteristics of increasing  $E_{eq}$  with  $\sigma_1$  for different temperatures are very similar. For this reason, averaging the  $m$  values was attempted and the averaged  $m$  value ( $m_{avg}$ ) of 0.624 was obtained. Then, regression analysis was re-performed for different

temperatures using Eq. (2) but with the fixed value of  $m = m_{avg}$ , as shown in Fig. 9b). The coefficient of determination ( $R^2$ -value) value for each respective temperature is also shown in Fig. 9b.

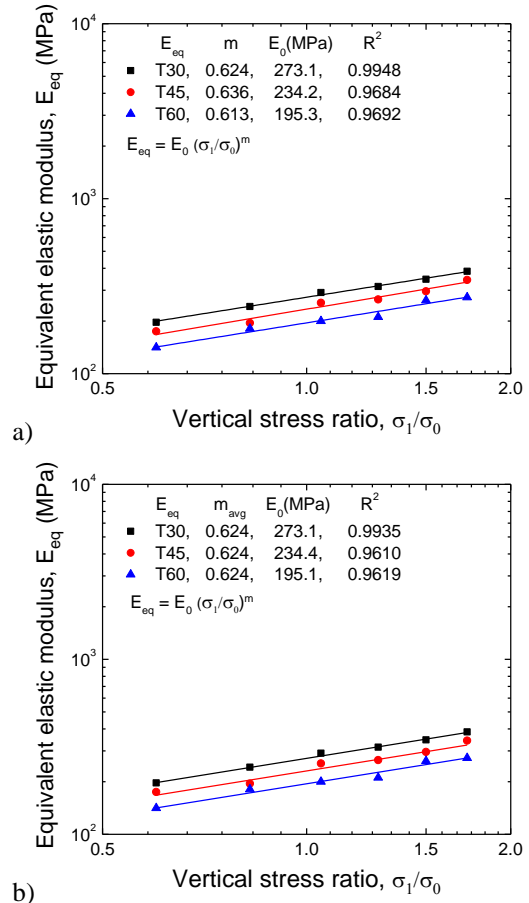


Fig. 9 Dependency of  $E_{eq}$  on the stress level and temperature with respective trend lines fitted by using: a) respective  $m$  values; and b) common averaged  $m$  value.

### 5.4 Creep Deformation

Fig. 10 shows the time histories of creep strain during 3-hr SL at different stress levels for the temperature equal to 30 °C. The trend of increasing creep axial strain with increasing stress ratio is noticed.

Fig. 11a) and 11b) compare the time histories of creep strain with different temperatures at the  $R$  values equal to 2.0 and 5.75, respectively. These  $R$  values are respectively the lowest and highest stress ratio levels employed for SL in the present study. It is seen from these figures that the creep strain increases with an increase in the temperature. In summary, it can be implied that under otherwise the same controlled conditions, the creep strain increases with increasing stress levels approaching the failure and

the temperature surrounding the sand.

Fig. 12 compares the creep strains at the end of 3-hr SL for different  $R$  values at which the SL was performed and different temperatures. The trend of increasing creep axial strain with an increase in the temperature as well as with an increase in the stress level can be seen. However, it can be seen that the stress level has more influence than the temperature on creep strain.

Creep strains at the end of sustained loading for 3 hours at different stress ratio levels from a)-SL-CL and b)-SL-CL tests with respective temperatures were compared. The trend of increasing creep axial strain with an increase in temperature can be seen. However, it is seen that the stress ratio level has a larger influence than the temperature on the creep strain development.

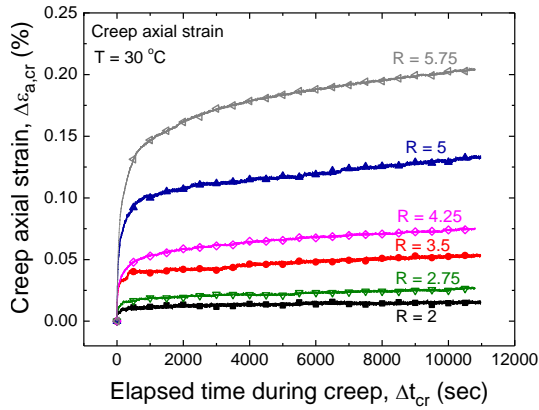


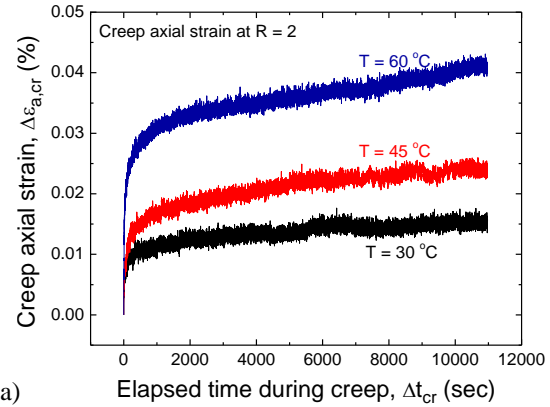
Fig. 10 Time histories of creep strain by 3-hr SL at different stress levels for the temperature equal to 30 °C.

## 6. CONCLUSIONS

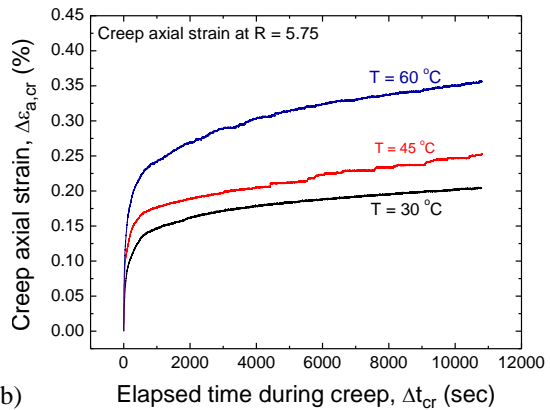
The following conclusions can be derived from the triaxial compression test results of the studied sand.

1. A newly triaxial loading apparatus that can accurately control both the loading and temperature histories in an automated manner was successfully developed.
2. With increasing temperature, the internal friction angles both at the peak and residual states decrease. In addition, the stress-strain characteristics by continuous ML degrade.
3. With increasing stress levels, the  $E_{eq}$  value significantly increases, exhibiting a hypo-elastic behavior. On the other hand, by comparing at the same stress level, the  $E_{eq}$  value noticeably decreases with increasing temperature.
4. Creep strain increases with increasing the stress

level and the temperature. The effect of stress level on the creep strain development seems to be more dominant than that of temperature.



a)



b)

Fig. 11 Comparison of time histories of creep axial strain for different temperatures by SL performed at  $R$  equal to a) 2.0; and b) 5.75.

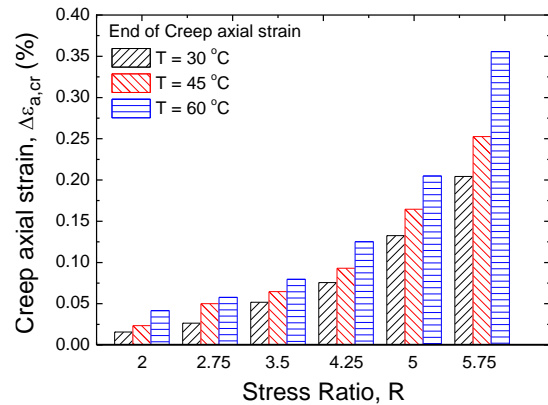


Fig. 12 Comparison of creep strain at the end of 3-hr SL for different stress ratio levels and temperatures.

## 7. ACKNOWLEDGMENTS

The authors would like to express their gratitude for financial support from King Mongkut's University of Technology Thonburi (KMUTT)

through The Petchra Pra Jom Klao Ph.D. scholarship under contract Grant No. 3/2559.

## 8. REFERENCES

- [1] Gens, A., Sánchez, M., Guimarães, L.D.N., Alonso, E.E., Lloret, A., Olivella, S., Villar, M.V. and Huertas, F., A Full-Scale in Situ Heating Test for High-Level Nuclear Waste Disposal: Observations, Analysis and Interpretation, *Géotechnique*, Vol. 59, No. 4, 2009, pp.377-399.
- [2] Brandon, T.L., Mitchell, J.K. and Cameron, J.T., Thermal Instability in Buried Cable Backfills. *Journal of Geotechnical Engineering*, Vol. 115, No. 1, 1989, pp.38-55.
- [3] Knellwolf, C., Peron, H. and Laloui, L., Geotechnical Analysis of Heat Exchanger Piles. *Journal of Geotechnical and Geoenvironmental Engineering*, Vol.137, Issue 10, 2011, pp.890-902.
- [4] Liu, H.L., Wang, C.L., Kong, G.Q., Ng, C.W. and Che, P., Model Tests on Thermo-Mechanical Behavior of an Improved Energy Pile. *European Journal of Environmental and Civil Engineering*, Vol. 22, No. 10, 2018, pp.1257-1272.
- [5] Olgun, C.G., and McCartney, J.S., Outcomes from International Workshop on Thermoactive Geotechnical Systems for Near-Surface Geothermal Energy: from Research to Practice. *DFI Journal-The Journal of aep Foundations Institute*, Vol. 8, Issue 2, 2014, pp.59-73.
- [6] Coccia, C.J., and McCartney, J.S., Impact of Heat Exchange on the Thermo-Hydro-Mechanical Response of Reinforced Embankments. In *Geo-Congress 2013: Stability and Performance of Slopes and Embankments III*, 2013, pp. 343-352.
- [7] Stewart, M.A., Coccia, C.J. and McCartney, J.S., Issues in the Implementation of Sustainable Heat Exchange Technologies in Reinforced, Unsaturated Soil Structures. In *Geo-Congress 2014: Geo-characterization and Modeling for Sustainability*, 2014, pp. 4066-4075.
- [8] Brandl, H., Energy Foundations and Other Thermo-Active Ground Structures. *Géotechnique*, Vol. 56, No. 2, 2006, pp.81-122.
- [9] Kertesz, R. and Sansalone, J., Hydrologic Transport of Thermal Energy from Pavement. *Journal of Environmental Engineering*, Vol. 140, No. 8, 2014, p.04014028.
- [10] Tatsuoka, F., Tateyama, M., Koda, M., Kojima, K.I., Yonezawa, T., Shindo, Y., and Tamai, S.I., Research and Construction of Geosynthetic-Reinforced Soil Integral Bridges. *Transportation Geotechnics*, Vol. 8, 2016, pp.4-25.
- [11] Gens, A., Soil-Environment Interactions in Geotechnical Engineering. *Géotechnique*, Vol. 60, No. 1, 2010, pp.3-74.
- [12] Tidfors, M. and Sällfors, G., Temperature Effect on Preconsolidation Pressure. *Geotechnical Testing Journal*, Vol. 12, No. 1, 1989, pp.93-97.
- [13] Cekerevac, C. and Laloui, L., Experimental Study of Thermal Effects on the Mechanical Behaviour of a Clay. *International journal for numerical and analytical methods in geomechanics*, Vol. 28, Issue 3, 2004, pp.209-228.
- [14] Tang, A.M., Cui, Y.J. and Banel, N., Thermo-Mechanical Behaviour of a Compacted Swelling Clay. *Géotechnique*, Vol.58, No. 1, 2008, pp.45-54.
- [15] Di Donna, A., and Laloui, L., Response of Soil Subjected to Thermal Cyclic Loading: Experimental and Constitutive Study. *Engineering Geology*, 190, 2015, pp.65-76.
- [16] Burland, J.B., Ninth Laurits Bjerrum Memorial Lecture: "Small is beautiful"-the Stiffness of Soils at Small Strains. *Canadian geotechnical journal*, Vol. 26, No. 4, 1989, pp.499-516.
- [17] Tatsuoka, F. and Kohata, Y., Stiffness of Hard Soils and Soft Rocks in Engineering Applications. In *Pre-Failure Deformation of Geomaterials. Proceedings of The International Symposium, 12-14 September 1994, Sapporo, Japan. 2 Vols.* 1995.
- [18] Kohata, Y., Tatsuokaj, F., Wang, L., Jiang, G.L., Hoque, E., and Kodaka, T., Modelling the Non-Linear Deformation Properties of Stiff Geomaterials. *Geotechnique*, Vol. 47, No.3, 1997, pp.563-580.
- [19] Hicher, P.Y., Elastic Properties of Soils. *Journal of Geotechnical Engineering*, Vol. 122, No. 8, 1996, pp.641-648.
- [20] Tatsuoka, F., Di Benedetto, H., Enomoto, T., Kawabe, S. and Kongkitkul, W., Various Viscosity Types of Geomaterials in Shear and Their Mathematical Expression. *Soils and Foundations*, Vol. 48, No. 1, 2008, pp.41-60.
- [21] Lu, R., Cheng, C., Nagel, T., Milsch, H., Yasuhara, H., Kolditz, O. and Shao, H., What Process Causes the Slowdown of Pressure Solution Creep. *Geomechanics and Geophysics for Geo-Energy and Geo-Resources*, Vol. 7, Issue 3, 2021, pp.1-11.
- [22] Liu, H., Liu, H., Xiao, Y. and McCartney, J.S., Effects of Temperature on the Shear Strength of Saturated Sand. *Soils and Foundations*, Vol. 58, No. 6, 2018, pp.1326-1338.
- [23] He, S.H., Shan, H.F., Xia, T.D., Liu, Z.J., Ding, Z. and Xia, F., The Effect of Temperature on the Drained Shear Behavior of Calcareous Sand. *Acta Geotechnica*, Vol. 16, Issue 2, 2021, pp.613-633.
- [24] Santucci De Magistris, F., Koseki, J., Amaya, M., Hamaya, S., Sato, T. and Tatsuoka, F., A Triaxial Testing System to Evaluate Stress-Strain Behavior of Soils for Wide Range of Strain and Strain Rate. *Geotechnical Testing Journal*, Vol.

- 22, No. 1, 1999, pp.44-60
- [25] Miura, S. and Toki, S., A Sample Preparation Method and Its Effect on Static and Cyclic Deformation-Strength Properties of Sand. *Soils and foundations*, Vol.22, No. 1, 1982, pp.61-77.
- [26] Shibuya, S., Tatsuoka, F., Teachavorasinskun, S., Kong, X.J., Abe, F., KIM, Y. and PARK, C., Elastic Deformation Properties of Geomaterials. *Soils and Foundations*, Vol.32, No. 3, 1992, pp.26-46.
- [27] Tatsuoka, F., Sato, T., Park, C.S., Kim, Y.S., Mukabi, J.N. and Kohata, Y., Measurements of Elastic Properties of Geomaterials in Laboratory Compression Tests. *Geotechnical Testing Journal*, Vol. 17, No. 1, 1994, pp.80-94.
- [28] Hoque, E. and Tatsuoka, F., Anisotropy in Elastic Deformation of Granular Materials. *Soils and foundations*, Vol. 38, No. 1, 1998, pp.163-179.

---

Copyright © Int. J. of GEOMATE All rights reserved, including making copies unless permission is obtained from the copyright proprietors.

---